

Physics-Incorporated Convolutional Recurrent Neural Networks for Source Identification and Forecasting of Dynamical Systems

Priyabrata Saha ¹

Saurabh Dash ¹

Saibal Mukhopadhyay ¹

Abstract

Spatio-temporal dynamics of physical processes are generally modeled using partial differential equations (PDEs). Though the core dynamics follows some principles of physics, real-world physical processes are often driven by unknown external sources. In such cases, developing a purely analytical model becomes very difficult and data-driven modeling can be of assistance. In this paper, we present a hybrid framework combining physics-based numerical models with deep learning for source identification and forecasting of spatio-temporal dynamical systems with unobservable time-varying external sources. We formulate our model PhICNet as a convolutional recurrent neural network (RNN) which is end-to-end trainable for spatio-temporal evolution prediction of dynamical systems and learns the source behavior as an internal state of the RNN. Experimental results show that the proposed model can forecast the dynamics for a relatively long time and identify the sources as well.

1 Introduction

Understanding the behavior of dynamical systems is a fundamental problem in science and engineering. Classical approaches of modeling dynamical systems involve formulating ordinary or partial differential equations (ODEs or PDEs) based on various physical principles, profound reasoning, intuition, knowledge and verifying those with experiments and observations. Recent successes of ma-

chine learning methods in complex sequence prediction tasks along with development in sensor technologies and computing systems motivate to predict the evolution of dynamical system directly from observation data without rigorous formalization and experiments by human experts [1, 2, 3, 4, 5, 6, 7]. Consequently, a number of machine learning models which incorporate knowledge from physics or applied mathematics, have been introduced for modeling complex dynamical systems [8, 9, 10, 11, 12, 13].

Real-world dynamical systems are often subjected to perturbation from time-varying external sources. Figure 1(a) shows an example where an elastic membrane under tension is being perturbed with an independent time-varying pressure. The undulation of the membrane can be observed as a regularly sampled spatiotemporal sequence. However, the spatiotemporal variation in the source term is often not known and not observable; but it couples with the wave propagation system to determine the undulation in the membrane. Moreover, although the basic governing dynamics (wave equation) of the system is known, the physical parameters such as propagation speed in that particular medium are often unknown. In such scenarios, we need to be able to predict spatiotemporal evolution of dynamical systems from partial knowledge of the governing dynamics and limited observability of the factors that influence the system behaviors.

In this paper, we consider to model a generic PDE-based dynamical system which is perturbed with external sources that follow another independent dynamics. Our goal is to design a neural network model that can be used for long-term predic-

¹School of Electrical and Computer Engineering, Georgia Institute of Technology, Atlanta, USA. Correspondence to: Priyabrata Saha <priyabratasaha@gatech.edu>

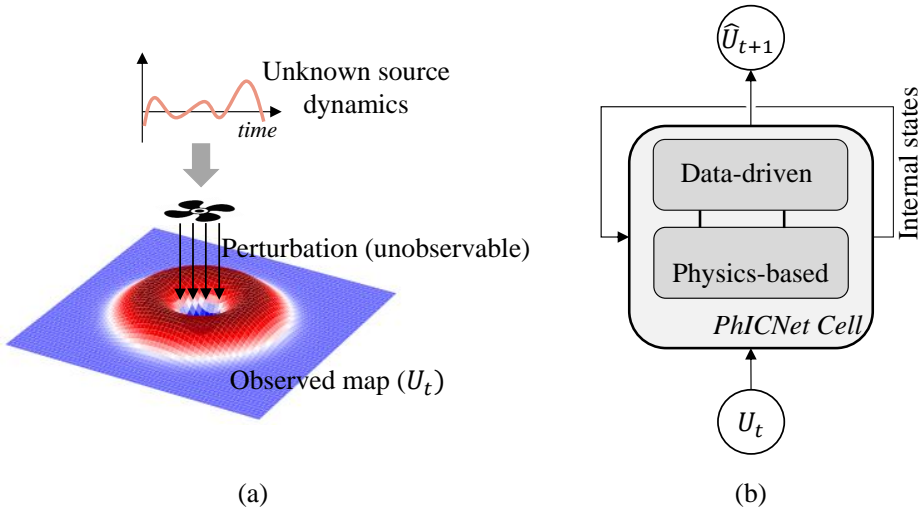


Figure 1: (a): An example dynamical system governed by partially-known PDE and unknown source dynamics. (b): High-level diagram of the recurrent network cell that is used to model such dynamics. Unobservable perturbation is learned as an internal state of PhICNet cell.

tion of the entire systems, as well as of the source dynamics. We assume the physical quantity that follows the combined dynamics can be observed as regularly sampled spatiotemporal sequence, but the source or perturbation is not observable separately. It is further assumed that we know what type of system we are observing and therefore scientific knowledge of such system can be incorporated in the model. In particular, we assume that the analytical form the underlying PDE is known *a priori*, *but the physical parameters of the system are unknown*.

We propose **Physics-Incorporated Convolutional Recurrent Neural Networks** (PhICNet) that combine physical models with data-driven models to learn the behavior of dynamical systems with unobservable time-varying external source term. Figure 1(b) shows the high-level diagram of a PhICNet cell. The basic concept of PhICnet is based on two key contributions. First, a generic homogeneous PDE of any temporal order can be mapped into a recurrent neural network (RNN) structure with trainable physical parameters. Second, the basic RNN structure for homogeneous PDE can be modified and integrated with a residual encoder-decoder network to identify and learn the source dynamics. The RNN structure stores the homogeneous solution of the underlying PDE as an internal state which is then compared with the input (observation) at the next step to find out if there exists

some source term or perturbation. The residual encoder-decoder network learns to propagate the source term as it is in case of constant perturbation or predict its progress in case of dynamic perturbation. The PhICNet cell stores the estimated perturbation or source term as an internal cell which can be used to understand behaviour of source dynamics. The integrated model can be trained end-to-end using stochastic gradient descent (SGD) based backpropagation through time (BPTT) algorithm.

Few existing models in literature can be used or extended to perform the spatiotemporal sequence prediction of dynamical systems with time-varying independent source. Pure data-driven models like ConvLSTM [3], residual networks [14, 15] can be used directly, but these models lack consideration of underlying physical dynamics resulting in limited accuracy. Furthermore, these pure data-driven models cannot identify the source dynamics separately. Deep hidden physics models (DHPM) [10] can model the underlying homogeneous PDE, but does not consider any nonlinear source term. A polynomial approximation can be added in DHPM to model nonlinear internal source. This strategy is used in PDE-Net [11] to incorporate nonlinear source term; however they consider only internal source term that is a nonlinear function of the observed physical quantity. DHPM, PDE-Net only consider PDEs that are first-order in time, although can be extended to model higher temporal order

systems if we know the temporal order a priori.

Our approach fundamentally differs from the past approaches as we model the system as an RNN that couples the known and unknown dynamics within the hidden cells and enables end-to-end training. We evaluate our model along with other baselines for two types of dynamical systems: a heat diffusion system and a wave propagation system. Experiments show that our model provides more accurate prediction compared to the baseline models. Furthermore, we show that our model can predict the source dynamics separately which is not possible with other models.

2 Related Work

2.1 RNNs for Dynamical Systems

Several studies have interpreted RNNs as approximation of dynamical systems [16, 17, 18, 19]. Recently, a number of RNN architectures have been proposed for data-driven modeling of dynamical systems. Trischler and D’Eleuterio [20] proposed an algorithm for efficiently training RNNs to replicate dynamical systems and demonstrated its capability to approximate attractor dynamical systems. A class of RNNs, namely Tensor-RNNs, has been proposed in [21, 22] for long-term prediction of nonlinear dynamical systems. Yeo and Melnyk [23] use LSTM for long-term prediction of nonlinear dynamics.

2.2 Learning PDEs from Data

Recently, numerous attempts have been made on data-driven discovery of PDE-based dynamical systems. Schaeffer [8], Rudy et al.[9] use sparse optimization techniques to choose the best candidates from a library of possible partial derivatives of the unknown governing equations. Raissi and Karniadakis [24] proposed a method to learn scalar parameters of PDEs using Gaussian process. A deep neural network is introduced in [25] to approximate the solution of a nonlinear PDE. The predicted solution is then fed to a physics-informed neural network to validate that solution. The physics-informed neural network is designed based on the explicit form of the underlying PDE which is assumed to be known except for a few scalar learnable parameters. Raissi [10] extended [25] to replace the known PDE-based neural network to a

generalized neural network which discovers the dynamics of underlying PDE using predicted solution and its derivatives. The inputs of the neural network are the partial derivatives up to a maximum order which is considered as a hyperparameter. Long et al. [11] introduced PDE-Net that uses trainable convolutional filters to perform differentiations. Filters are initialized as differentiating kernels of corresponding orders, and trained by imposing some constraints to maintain differentiating property. They assumed that the maximum order of derivative is known a priori. In PDE-Net 2.0 [26], a symbolic neural network is integrated with original PDE-Net to uncover more complex analytical form. de Bezenac et al. [13] proposed a convolutional neural network (CNN) that incorporates prior scientific knowledge for the problem of forecasting sea surface temperature. They design their model based on the general solution of the advection-diffusion equation. Long et al. [12] studied a problem similar to ours where the source or perturbation term of the PDE follows another dynamics. They mapped the known PDE into a cellular neural network with trainable physical parameters and integrate that with ConvLSTM [3] that models the source dynamics. However, they assumed that the source or perturbation is observable and they train the two networks separately.

3 Problem Description

We consider dynamical systems governed by the following generic inhomogeneous PDE

$$\begin{aligned} \frac{\partial^n u}{\partial t^n} = & F\left(x, y, u, \frac{\partial u}{\partial x}, \frac{\partial u}{\partial y}, \frac{\partial^2 u}{\partial x^2}, \frac{\partial^2 u}{\partial x \partial y}, \frac{\partial^2 u}{\partial y^2}, \dots; \theta\right) \\ & + v(x, y, t), \quad (x, y) \in \Omega \subset \mathbb{R}^2, t \in [0, T]. \end{aligned} \quad (1)$$

$u(x, y, t) \in \mathbb{R}$ is the observed physical quantity at the spatial location $(x, y) \in \Omega$ at time $t \in [0, T]$. θ corresponds to the physical parameters of the system. For example, if we are studying a diffusive system, then θ corresponds to the diffusivity of the medium. $v(x, y, t) \in \mathbb{R}$ is the source term or perturbation at location $(x, y) \in \Omega$ at time $t \in [0, T]$ which is governed by another independent dynamics delineated by:

$$\frac{\partial^k v}{\partial t^k} = G(x, y, v) \quad (2)$$

Our goal is to learn the spatiotemporal evolution of the source or perturbation (i.e. v) as well as of the system jointly defined by equation 1 and equation 2 while observing only u .

Assumptions We make following assumptions about the problem:

- We have the *a priori* knowledge about what type of physical quantities we are observing and how such system behave in absence of any external perturbation or source. In other words, we know the analytical form of function F and the temporal order n .
- Physical parameters of the system θ are not known.
- The perturbation v is not observable or cannot be computed directly from the observed quantity u as θ is unknown. The temporal order of the perturbation or source dynamics is either known or can be chosen as a hyperparameter.

This problem can be formulated as a spatiotemporal sequence prediction problem. Suppose the observation space is discretized into a $X \times Y$ grid and $U_t \in \mathbb{R}^{X \times Y}$ is the observed map at timestep $t \in \{0, 1, \dots, T\}$. We aim to design a physics-incorporated convolutional-RNN \mathcal{R} :

$$\hat{U}_{t+1} = \mathcal{R}(\hat{U}_t, \dots, \hat{U}_{t-n-k+1}), \quad t \in \{n+k-1, \dots, T-1\} \quad (3)$$

such that $\sum_{t=n+k}^T \mathcal{L}(U_t, \hat{U}_t)$ is minimized. \hat{U}_t is the predicted map at timestep $(t-1)$ and $\hat{U}_t = U_t \quad \forall t \in \{0, \dots, n+k-1\}$. \mathcal{L} is the loss function between observed map and predicted map. It is noteworthy that we need $(n+k)$ previous maps, instead of just n , to predict the next map in an n^{th} order (temporal) system because the source/perturbation is unknown and source follows a k^{th} order dynamics.

4 The PhICNet Model: Foundation and Design

4.1 Background on Recurrent Neural Networks

The recurrent neural network (RNN) is an elegant generalization of feedforward neural networks to incorporate temporal dynamics of data [27, 28, 29]. The RNN and its various evolved topologies have

proven efficacious in numerous sequence modelling tasks [30, 31, 32, 1, 3]. At each time step, an input vector i_t is fed to the RNN. The RNN modifies its internal state h_t based on the current input and previous internal state. The updated internal state is then used to predict the output o_t . The following set of equations (equation 4) delineates the computation inside a standard RNN.

$$\begin{aligned} h_t &= \sigma_h(W_{hi}i_t + W_{hh}h_{t-1} + b_h) \\ o_t &= \sigma_o(W_{oh}h_t + b_o) \end{aligned} \quad (4)$$

W_{hi}, W_{hh}, W_{oh} are the weight matrices of the RNN and b_h, b_o are bias vectors. σ_h and σ_o are nonlinear activation functions. Temporal update in the internal state allows the RNN to make use of past information while predicting the current output.

The input i_t , internal state h_t and output o_t of standard RNN are all 1D vectors and the operations are fully-connected. To deal with 2D image data, Xingjian et al. proposed convolutional LSTM [3] that uses convolutional operations instead of fully-connected operations of standard LSTM [32], an evolved variant of the RNN. Incorporating convolutional operations in RNN, we can write the computation inside a convolutional-RNN as follows:

$$\begin{aligned} H_t &= \sigma_h(W_{hi} * I_t + W_{hh} * H_{t-1} + b_h) \\ O_t &= \sigma_o(W_{oh} * H_t + b_o) \end{aligned} \quad (5)$$

where, I_t , H_t and O_t are the input, internal state and output, respectively, of the convolutional-RNN at time step t and are all 2D images. ‘*’ denotes the convolution operator.

4.2 Proposed RNN Model for Generic Homogeneous PDE

Figure 2(a) illustrates the structure of the RNN we propose for modeling a generic homogeneous PDE (i.e. zero source term); we will refer the model as PDE-RNN. Inputs to the RNN cell are 2D observation maps $U_t \in \mathbb{R}^{X \times Y}, t \in \{0, \dots, T\}$. The RNN cell keeps an memory that stores the past information required for current step prediction. The concept of cell memory was introduced in LSTM [32]. Cell memory in LSTM is controlled by several self-parameterized gates to learn what information to store and what information to forget. In contrast, past information required to be stored in the cell memory in our physics-incorporated RNN is completely determined beforehand based on the known

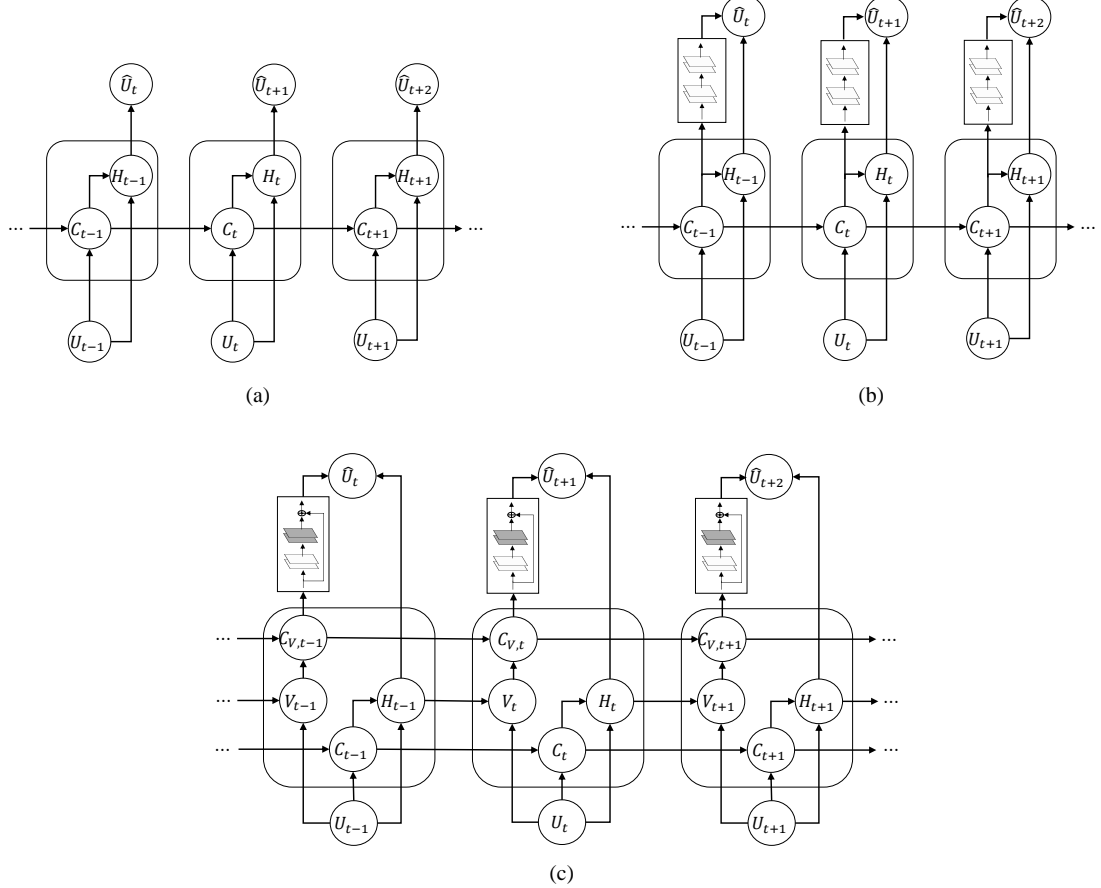


Figure 2: (a): PDE-RNN: RNN structure (unfolded) that maps a generic homogeneous PDE. U_t is the observed map at time step t and \hat{U}_{t+1} is the prediction of the next map. H_t and C_t are internal states of the RNN representing the homogeneous solution and cell memory, respectively. For homogeneous PDE, $\hat{U}_{t+1} = H_t$. (b): PDE-RNN + CNN: a corrective convolutional module is added with the homogeneous solution to incorporate the source term or perturbation. (c): PhICNet: Proposed RNN structure that models the dynamical system with time-varying independent source. A residual encoder-decoder network, which models the source dynamics, is integrated with (a). V_t stores the estimated perturbation. $C_{V,t}$ is the cell memory for storing past estimated perturbation maps.

temporal order n (in equation 1) of the observed system. For an n^{th} order (temporal) system, the cell memory stores the current and past $(n-1)$ observed maps. At time step t , the state of the cell memory (we will call it cell state from now on) C_t defined by the following equation

$$C_t = [U_t, \dots, U_{t-n+1}] \quad (6)$$

where $[\cdot]$ denotes the concatenation operation along a new dimension. The cell state can be seen as a 3D tensor ($C_t \in \mathbb{R}^{n \times X \times Y}$). Cell state at current time step t can be written as a function of previous cell state C_{t-1} and current input U_t :

$$C_t = W_{cc} \odot C_{t-1} + w_{cu} \circ U_t \quad (7)$$

W_{cc} is a 2D square matrix of order n and the $(p, q)^{th}$ element of W_{cc} , $p \in \{1, \dots, n\}$ and $q \in \{1, \dots, n\}$, is defined as follows.

$$W_{cc}^{pq} = \begin{cases} 1 & \text{if } p = q + 1 \\ 0 & \text{otherwise} \end{cases} \quad (8)$$

‘ \odot ’ denotes a matrix-tensor product resulting in a tensor $\tilde{C} \in \mathbb{R}^{n \times X \times Y}$ such that

$$\tilde{C}^p = \sum_{q=1}^n W_{cc}^{pq} C_{t-1}^q, \quad p \in \{1, \dots, n\}. \quad (9)$$

The operator \circ between 2D observation map $U_t \in \mathbb{R}^{X \times Y}$ and 1D vector $w_{cu} = [1, 0, \dots, 0]^T \in \mathbb{R}^n$

performs a vector-matrix product to yield a tensor $\hat{C} \in \mathbb{R}^{n \times X \times Y}$ such that

$$\hat{C}^p = w_{cu}^p U_t, \quad p \in \{1, \dots, n\}. \quad (10)$$

Cell state C_t and input U_t are used to compute $H_t \in \mathbb{R}^{X \times Y}$ as follows.

$$\begin{aligned} H_t = & w_{hc} \odot C_t \\ & + f(U_t, D_{10} * U_t, D_{01} * U_t, D_{11} * U_t, \dots; \theta) \end{aligned} \quad (11)$$

$w_{hc} \in \mathbb{R}^n$ is determined by the temporal order of the dynamics. The elements of w_{hc} are the coefficients of past observation maps in the finite difference approximation of $\frac{\partial^n}{\partial t^n}$ and are given by the following equation.

$$w_{hc}^p = (-1)^{p+1} \binom{n}{p}, \quad p \in \{1, \dots, n\} \quad (12)$$

‘ \odot ’ denotes a vector-tensor product resulting in a 2D matrix $\tilde{H} \in \mathbb{R}^{X \times Y}$ such that

$$\tilde{H} = \sum_{p=1}^n w_{hc}^p C_t^p \quad (13)$$

Function f (in equation 11) is the implementation of F (in equation 1) for discretized observation maps. As mentioned in section 3, the analytical form of F or f is known to us, but the physical parameters θ are unknown and trainable. Spatial derivatives of observation map U_t are computed as convolution with differential kernels. D_{jl} denotes the differential kernel corresponds to $\frac{\partial^{j+l}}{\partial x^j \partial y^l}$. The size and elements of a differential kernel are determined by the finite difference approximation of corresponding derivative. H_t represents the solution of the system that is governed by a homogenous PDE. In other words, H_t corresponds to the predicted map at timestep t when there is no source term or perturbation.

4.3 Approach to Incorporate Source Dynamics

The basic structure of RNN for homogeneous PDE (PDE-RNN) needs to be modified to incorporate dynamic source term. A simple modification can be adding a convolutional neural network (CNN) with the PDE-RNN. We will call this modified structure (Figure 2(b)) PDE-RNN + CNN. The convolutional network takes the cell state C_t as input and

add a corrective term, which accounts for the source or perturbation, to the homogeneous solution. Although PDE-RNN + CNN incorporates the known PDE in its structure, it does not get much benefit in forecasting the system or identifying the source dynamics as we will show in section 5.

In contrast to directly predicting a correcting term from observation maps like PDE-RNN + CNN, we propose to estimate an intermediate source map and use that to learn the source dynamics. Separating the source maps from the overall dynamics makes it easier to learn the source dynamics. Figure 2(c) shows the proposed PhICNet structure. An internal state V_t is added in the cell that estimates the perturbation using the predicted homogeneous solution from the previous step and the current input. $V_t \in \mathbb{R}^{X \times Y}$ is computed as follows.

$$V_t = U_t - H_{t-1} \quad (14)$$

Another cell memory $C_{V,t}$ is added to store past perturbation estimates. Assuming a K^{th} order source dynamics, $C_{V,t}$ can be seen as a 3D tensor ($C_{V,t} \in \mathbb{R}^{K \times X \times Y}$) given by:

$$C_{V,t} = [V_t, \dots, V_{t-K+1}] \quad (15)$$

Cell memory $C_{V,t}$ is updated at each time step by the following equation.

$$C_{V,t} = W_{ccv} \odot C_{V,t-1} + w_{cv} \circ V_t \quad (16)$$

$W_{ccv} \in \mathbb{R}^{K \times K}$ and $w_{cv} \in \mathbb{R}^K$ have similar properties of W_{cc} and w_{cu} , respectively, of equivalent equation 7. Finally, the predicted map \hat{U}_{t+1} is computed by the following equation.

$$\hat{U}_{t+1} = H_t + w_{vc} \odot C_{V,t} + g(C_{V,t}) \quad (17)$$

Function g , the implementation of fuction G (in equation 2) for discretized source maps, captures the source dynamics. We use a residual convolutional network for this purpose such that

$$\hat{V}_{t+1} = w_{vc} \odot C_{V,t} + g(C_{V,t}) \quad (18)$$

$w_{vc} \odot C_{V,t}$ is a vector-tensor product similar to equation 13. The vector $w_{vc} \in \mathbb{R}^K$ is a trainable parameter and initialized with coefficients of the finite difference approximation of $\frac{\partial^K}{\partial t^K}$. \hat{V}_{t+1} is the predicted source map which is added to the homogeneous solution H_t to get the predicted map \hat{U}_{t+1} (equation 17).

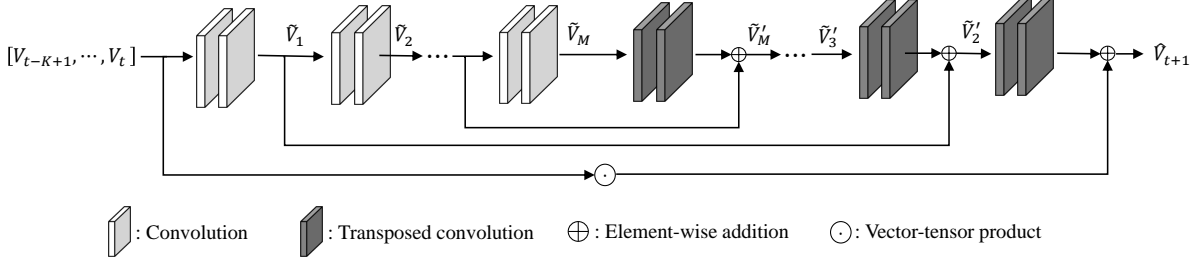


Figure 3: Architecture of the residual encoder-decoder network used for source dynamics modeling.

The motivation behind using residual network for modeling the source dynamics is that several studies have established the connection between residual networks and differential equations [33, 34, 35, 19]. We use an architecture similar to residual encoder-decoder network (RED-Net) [15]. To incorporate K^{th} order source dynamics, we use past K estimated source maps stacked across the channel dimension as input to RED-Net. Moreover, we add a weighted combination of past K estimated source maps $w_{vc} \odot C_{V,t}$, instead of adding just V_t , to the final output. The elements of w_{vc} are initialized with the coefficients of the finite difference approximation of $\frac{\partial^K}{\partial t^K}$.

Figure 3 shows the architecture of the residual encoder-decoder network with M convolutional and M transposed convolutional blocks. Each convolutional block consists of two convolutional layers. Similarly, each transposed convolutional block comprises two transposed convolutional layers. Convolutional encoder extracts feature at different scales. These feature maps are used by the transposed convolutional decoder with symmetric skip connections from corresponding convolutional block to capture dynamics at different scales. Skip connection also allows to use deeper network for complex dynamics without encountering the problem of vanishing gradient.

The computation at the m^{th} convolutional block is given by the following equation.

$$\begin{aligned} \tilde{V}_m &= \sigma(W_{m2} * \sigma(W_{m1} * \tilde{V}_{m-1})), \\ m &\in \{1, \dots, M\}, \\ \tilde{V}_0 &= C_{V,t} \end{aligned} \quad (19)$$

The computation at the m^{th} transposed convolutional block from the end is delineated by

$$\begin{aligned} \tilde{V}'_m &= \sigma(W'_{m2} * \sigma(W'_{m1} * \tilde{V}'_{m+1}) + \tilde{V}_{m-1}), \\ m &\in \{2, \dots, M\}, \\ \tilde{V}'_{M+1} &= \tilde{V}_M \end{aligned} \quad (20)$$

and,

$$\tilde{V}'_1 = W'_{12} * \sigma(W'_{11} * \tilde{V}'_2) + w_{vc} \odot \tilde{V}_0 \quad (21)$$

The predicted source map is given by $\hat{V}_{t+1} = \tilde{V}'_1$. $*$ denotes the transposed convolution operation and σ is the activation function ReLU.

4.4 Training Loss

For a sequence of observation maps $\{U_0, U_1, \dots, U_T\}$ and n^{th} order (temporal) system, assuming a K^{th} order source dynamics, the prediction loss is defined as follows.

$$\mathcal{L}_{pred} = \frac{1}{T - n - K + 1} \sum_{t=n+K}^T \|U_t - \hat{U}_t\|_2^2 \quad (22)$$

Estimated source map V_t , after observing U_t at timestep t , should match with predicted source map \hat{V}_t from previous timestep. Accordingly, we add a source prediction loss to the training objective, given by

$$\mathcal{L}_{source_pred} = \frac{1}{T - n - K + 1} \sum_{t=n+K}^T \|V_t - \hat{V}_t\|_2^2 \quad (23)$$

Furthermore, source map can be densely distributed or sparse (may contain only a single

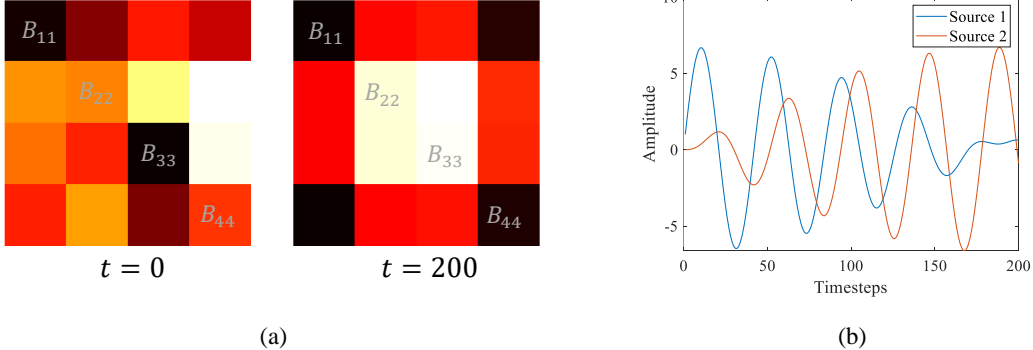


Figure 4: (a): Heat-source maps at the initial and final time step of an example sequence used in our experiment. (b): Temporal behavior of the coupled oscillators acting as sources in an example sequence used in our wave propagation experiment.

source). To deal with source map sparsity, we add a $L1$ penalty :

$$\mathcal{L}_{source_sparse} = \frac{1}{T - n - K + 1} \sum_{t=n+K}^T \|\hat{V}_t\|_1 \quad (24)$$

The overall loss for training is $\mathcal{L} = \mathcal{L}_{pred} + \mathcal{L}_{source_pred} + \lambda \mathcal{L}_{source_sparse}$, where λ is a hyper-parameter.

5 Experimental Evaluation

We evaluate our model on two dynamical systems: heat diffusion system and wave propagation system. Heat diffusion system has temporal order of 1, while wave propagation system is a second order system. For the task of forecasting of the overall dynamics, we compare the proposed model with PDE-RNN + CNN, ConvLSTM [3], a residual encoder-decoder network. However, among the baselines, only PDE-RNN + CNN can be used for source identification task.

In contrast to the residual encoder-decoder used in our model to predict only the source dynamics, the baseline residual encoder-decoder network (RED-Net) models the combined dynamics. Accordingly, the input and output of the baseline residual encoder-decoder network are observation maps (U). For RED-Net baseline, we assume the temporal order of the system is known a priori, i.e. for an n^{th} order system, assuming a K^{th} order source dynamics, input to the model is the sequence $\{U_t, U_{t-1}, \dots, U_{t-n-K+1}\}$ while predicting \hat{U}_{t+1} .

5.1 Heat Diffusion System

Heat diffusion at the surface of a material is described by:

$$\frac{\partial u}{\partial t} = \alpha \left(\frac{\partial^2 u}{\partial x^2} + \frac{\partial^2 u}{\partial y^2} \right) + v(x, y, t), \quad (x, y) \in \Omega \subset \mathbb{R}^2, t \in [0, T] \quad (25)$$

where $u(x, y, t)$ is the heat density at location (x, y) at time t and $v(x, y, t)$ is the perturbation due to heat source(s). α is the thermal diffusivity of the material. Equation 25 is one of the fundamental PDEs and is used to describe diffusion of heat, chemicals, brownian motion, diffusion models of population dynamics, and many other phenomena [36].

The computation space Ω is discretized into 64×64 regular mesh, i.e. $U_t \in \mathbb{R}^{64 \times 64}$. For heat-source, we consider the source map $V_t \in \mathbb{R}^{64 \times 64}$ is divided into 16 equal-sized blocks initialized with random values in $[0, 1]$. All grid points belonging to a block B_{jl} take same value at any time step. The evolution of source map happens in the block level. Each block B_{jl} follows a dynamics given by:

$$\frac{dV_t^{B_{jl}}}{dt} = \sum_{(r,s) \in \mathcal{N}(j,l)} \gamma (V_t^{B_{rs}} - V_t^{B_{jl}}) \quad (26)$$

where $V_t^{B_{jl}}$ denotes the value of block B_{jl} at timestep t , γ is a positive constant and $\mathcal{N}(j,l)$ represents the 4-connected neighborhood of block B_{jl} . Figure 4(a) shows an example of source map at the initial and final time step. Training and test dataset are generated using numerical solution

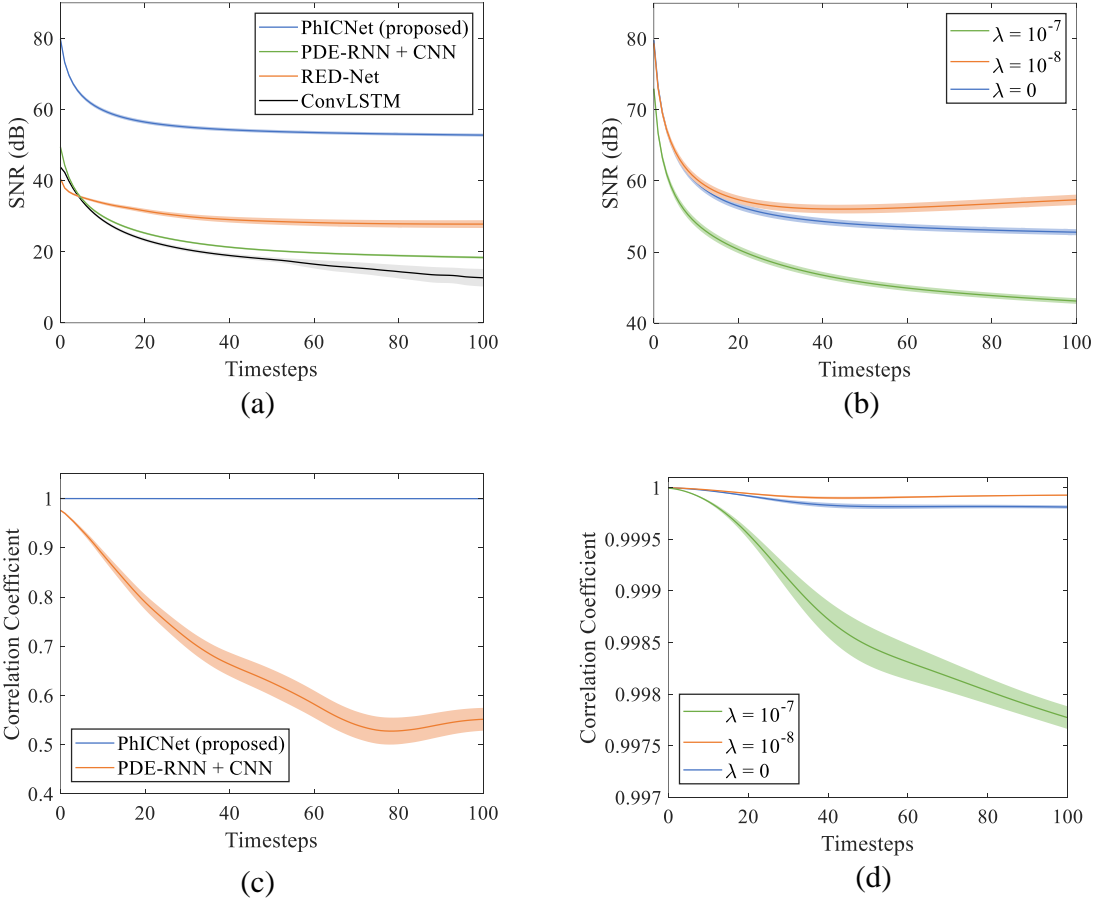


Figure 5: (a, c): Quantitative comparison of proposed PhICNet with respect to other baselines in the task of forecasting (a) and source identification (c) for the heat diffusion system. (b, d): Effect of sparsity hyperparameter λ on forecasting (b) and source identification (d) performance of the proposed model. In all plots, shaded areas show 95% confidence interval.

method starting from initial condition $U_{t<0} = 0$ and assuming homogeneous Dirichlet boundary condition. Each sequence is comprises 200 frames and the training set contains 100 such sequences while the test set contains 50.

In this system, the trainable parameters are diffusivity α and the parameters of the residual encoder-decoder network used to model the source dynamics. Since we need second-order spatial derivatives (equation 25), the minimum size of the corresponding differential kernels should be 3×3 . Specifically, following two differential kernels are used to compute H_t in equation 11.

$$D_{20} = \begin{pmatrix} 0 & 0 & 0 \\ 1 & -2 & 1 \\ 0 & 0 & 0 \end{pmatrix}, \quad D_{02} = \begin{pmatrix} 0 & 1 & 0 \\ 0 & -2 & 0 \\ 0 & 1 & 0 \end{pmatrix} \quad (27)$$

We use Signal-to-Noise Ratio (SNR), defined in equation 28, to quantitatively compare the perfor-

mance of different models in forecasting the overall dynamics.

$$SNR(U_t, \hat{U}_t) = 20 \log_{10} \frac{\|U_t\|_2}{\|U_t - \hat{U}_t\|_2} \quad (28)$$

However, SNR cannot be used as a metric for source map comparison. To compare two maps using SNR, both maps need to have values in very similar scale. Since the inputs to the models are normalized and the source maps are learned as intermediate states without any direct supervisory signal, the estimated maps do not match the scale of true source maps. To quantify the similarity between true and estimated source maps, we use Correlation Coefficient as metric. Correlation coefficient between estimated source map V_t and true source map $V_{true,t}$ is given by

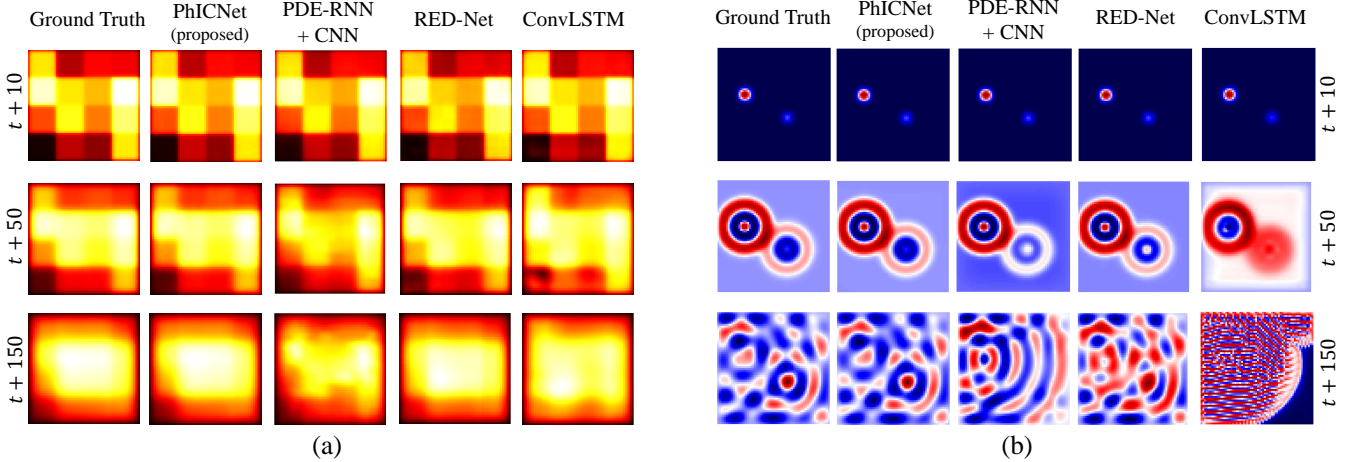


Figure 6: Qualitative comparison of predicted heat maps (a) and wave maps (b) by different models at time steps $t + 10$, $t + 50$ and $t + 150$ when last observation is taken at t .

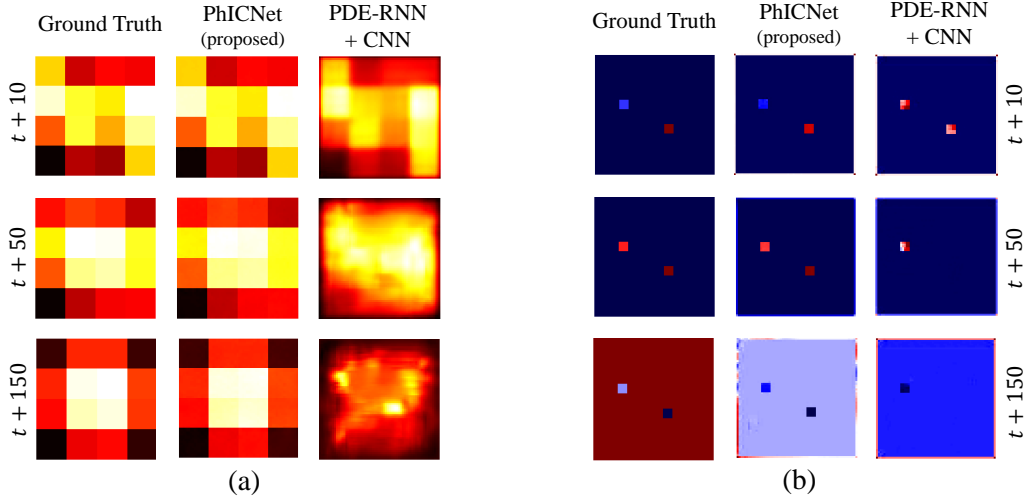


Figure 7: Qualitative comparison between true source maps and predicted source maps by proposed PhICNet and PDE-RNN + CNN for heat system (a) and wave system (b) at time steps $t + 10$, $t + 50$ and $t + 150$.

$$\begin{aligned} & \rho(V_{true,t}, V_t) \\ &= \frac{\sum_{j,l} (V_{true,t}^{jl} - \bar{V}_{true,t})(V_t^{jl} - \bar{V}_t)}{\left(\sum_{j,l} (V_{true,t}^{jl} - \bar{V}_{true,t})^2\right)^{1/2} \left(\sum_{j,l} (V_t^{jl} - \bar{V}_t)^2\right)^{1/2}} \end{aligned} \quad (29)$$

where \bar{V}_t and $\bar{V}_{true,t}$ denote the mean values of V_t and $V_{true,t}$ respectively.

Figure 5 shows the quantitative comparison of proposed method with respect to other baselines and choice of hyperparameter λ in the task of forecasting and source identification for the heat diffu-

sion system. Qualitative comparison of predicted heat maps by different models along with ground truth is depicted in Figure 6(a). PhICNet outperforms all the baselines. RED-Net is the best performing baseline. Effective modeling of dynamics by RED-Net is a key factor in the performance of our model as well since we use it for source dynamics modeling. Source maps predicted by the proposed model and PDE-RNN + CNN are compared with ground truth in Figure 7(a).

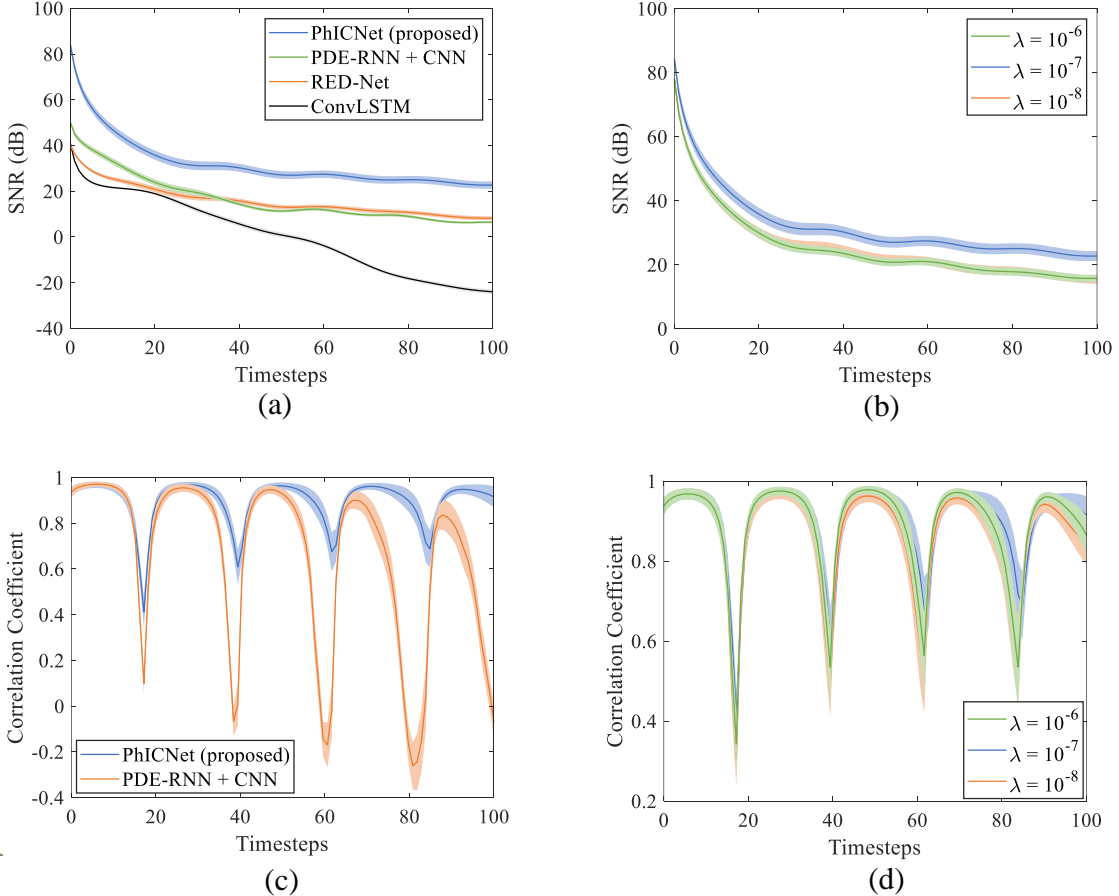


Figure 8: (a, c): Quantitative comparison of proposed PhICNet with respect to other baselines in the task of forecasting (a) and source identification (c) for the wave propagation system. (b, d): Effect of sparsity hyperparameter λ on forecasting (b) and source identification (d) performance of the proposed model. In all plots, shaded areas show 95% confidence interval.

5.2 Wave Propagation System

Undulation in a stretched elastic membrane due to some perturbation can be described by:

$$\frac{\partial^2 u}{\partial t^2} = c^2 \left(\frac{\partial^2 u}{\partial x^2} + \frac{\partial^2 u}{\partial y^2} \right) + v(x, y, t), \quad (x, y) \in \Omega \subset \mathbb{R}^2, t \in [0, T] \quad (30)$$

where $u(x, y, t)$ is the deflection at location (x, y) at time t and $v(x, y, t)$ is the external perturbation. c is the wave propagation speed. We consider two coupled oscillators at random locations as wave sources perturbing the membrane. Figure 4(b) shows an example of temporal behavior of the sources.

Similar to heat diffusion system, the computation space Ω is discretized into 64×64 regular mesh, i.e. $U_t \in \mathbb{R}^{64 \times 64}$. Unlike the source map considered for the heat system, the source map $V_t \in \mathbb{R}^{64 \times 64}$ for

this wave system is sparse as the perturbation is applied only at two small regions of the membrane. The initial amplitude and location of the oscillators are chosen randomly for each sequence in the dataset. Therefore, source identification task requires identifying both the location and strength of the sources. Training and test dataset are generated using numerical solution method starting from initial condition $U_{t < 0} = 0$ and assuming homogeneous Dirichlet boundary condition. Each sequence is comprises 200 frames and the training set contains 300 such sequences while the test set contains 50. Trainable parameters for this system include propagation speed c and the parameters of residual encoder-decoder network that is used to model the source dynamics. The differential kernels used for this system are same as equation 27.

Figure 8 shows the quantitative comparison of

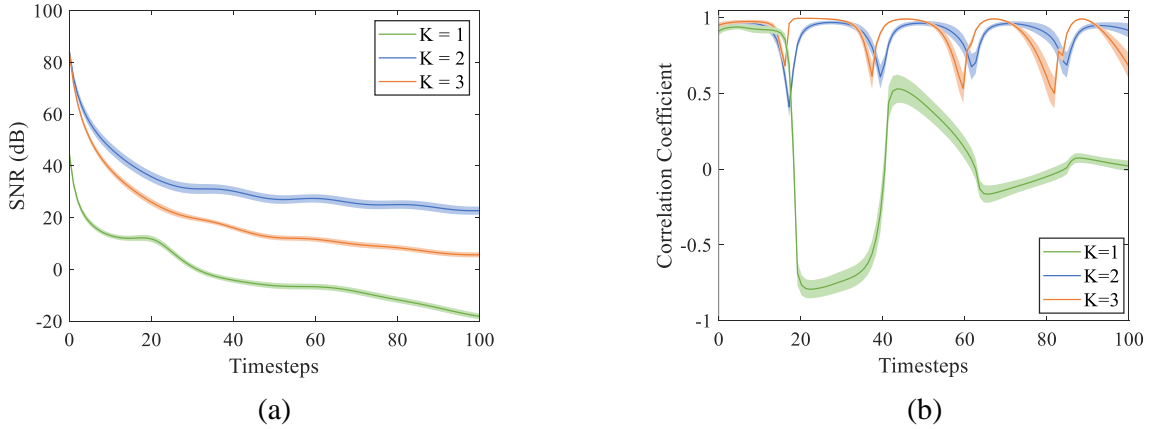


Figure 9: Choice of temporal order K in source dynamics modeling: effect on forecasting (a) and source identification (b) performance for the wave propagation system.

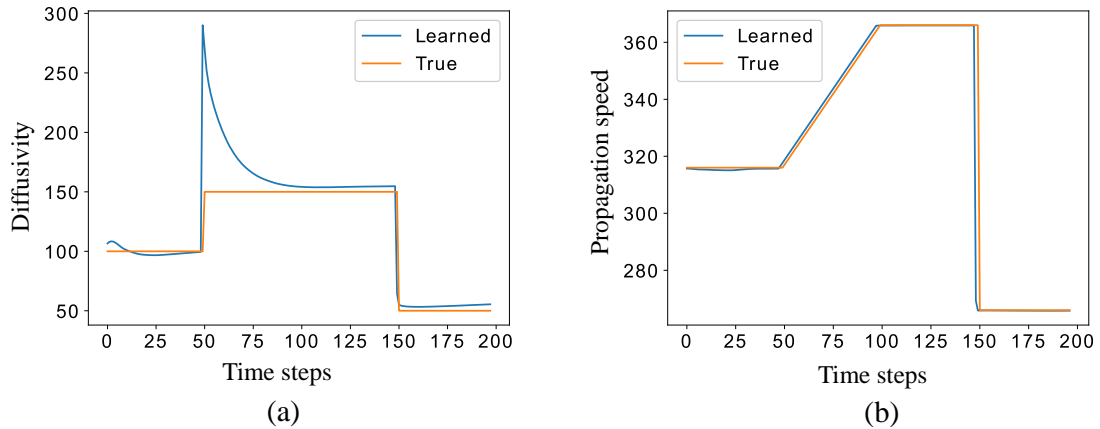


Figure 10: Online learning of time-varying physical parameters: diffusivity of heat diffusion system (a), propagation speed of wave propagation speed (b).

proposed method with respect to other baselines and choice of hyperparameter λ in the task of forecasting and source identification for the wave propagation system. Qualitative comparison of predicted maps by different models along with ground truth is depicted in Figure 6(b). Figure 7(b) compares the source maps predicted by the proposed model and PDE-RNN + CNN with ground truth.

Choice of temporal order K in source dynamics modeling Figure 9 compares the forecasting and source identification performance for different values of K (in equation 15). The true order of the source dynamics (coupled oscillators) of the wave propagation system is 2. Best performance is observed when the source order is exactly known, i.e. $K = 2$. Choosing an order higher than the true value ($K = 3$) is better compared to choosing an order lower than the true value ($K = 1$).

Proposed method with respect to other baselines and choice of hyperparameter λ in the task of forecasting and source identification for the wave propagation system. Qualitative comparison of predicted maps by different models along with ground truth is depicted in Figure 6(b). Figure 7(b) compares the source maps predicted by the proposed model and PDE-RNN + CNN with ground truth.

5.3 Online Learning of Time-varying Physical Parameters

In all aforementioned experiments, we have considered unknown but constant physical parameters which are learned in conjunction with unknown source dynamics. However, physical parameters of real-world physical systems are often not fixed and can change over time. In this experiment, we vary the physical parameter of the system over time and

investigate if the trained model can adapt with new values of the physical parameter online. At each time step, the current observation is used to re-tune the physical parameters of the system, while the other parameters are kept frozen. Figure 10 shows that our model can quickly adapt with changes in physical parameters.

6 Conclusion

We developed a physics-incorporated recurrent neural network PhICNet for spatiotemporal forecasting of dynamical systems with time-varying independent source. Besides forecasting the combined dynamics, our model is also capable of predicting the evolution of source dynamics separately. PhICNet is generalized to a class of partially known spatio-temporal dynamical systems driven by unknown source. It is possible to relax the assumption on knowledge of analytical form of the underlying PDE by allowing trainable convolution kernels like PDE-Net. We aim to investigate this as a future work. Learning the dynamics from non-spatiotemporal irregular observation will be an important extension as well.

References

- [1] I Sutskever, O Vinyals, and QV Le. Sequence to sequence learning with neural networks. *Advances in NIPS*, 2014.
- [2] Junyoung Chung, Caglar Gulcehre, KyungHyun Cho, and Yoshua Bengio. Empirical evaluation of gated recurrent neural networks on sequence modeling. *arXiv preprint arXiv:1412.3555*, 2014.
- [3] SHI Xingjian, Zhourong Chen, Hao Wang, Dit-Yan Yeung, Wai-Kin Wong, and Wang-chun Woo. Convolutional lstm network: A machine learning approach for precipitation nowcasting. In *Advances in neural information processing systems*, pages 802–810, 2015.
- [4] Chelsea Finn, Ian Goodfellow, and Sergey Levine. Unsupervised learning for physical interaction through video prediction. In *Advances in neural information processing systems*, pages 64–72, 2016.
- [5] Ankit Kumar, Ozan Irsoy, Peter Ondruska, Mohit Iyyer, James Bradbury, Ishaan Gulrajani, Victor Zhong, Romain Paulus, and Richard Socher. Ask me anything: Dynamic memory networks for natural language processing. In *International conference on machine learning*, pages 1378–1387, 2016.
- [6] Namhoon Lee, Wongun Choi, Paul Vernaza, Christopher B Choy, Philip HS Torr, and Manmohan Chandraker. Desire: Distant future prediction in dynamic scenes with interacting agents. In *Proceedings of the IEEE Conference on Computer Vision and Pattern Recognition*, pages 336–345, 2017.
- [7] Matthias Minderer, Chen Sun, Ruben Villegas, Forrester Cole, Kevin P Murphy, and Honglak Lee. Unsupervised learning of object structure and dynamics from videos. In *Advances in Neural Information Processing Systems*, pages 92–102, 2019.
- [8] Hayden Schaeffer. Learning partial differential equations via data discovery and sparse optimization. *Proceedings of the Royal Society A: Mathematical, Physical and Engineering Sciences*, 473(2197):20160446, 2017.
- [9] Samuel H Rudy, Steven L Brunton, Joshua L Proctor, and J Nathan Kutz. Data-driven discovery of partial differential equations. *Science Advances*, 3(4):e1602614, 2017.
- [10] Maziar Raissi. Deep hidden physics models: Deep learning of nonlinear partial differential equations. *The Journal of Machine Learning Research*, 19(1):932–955, 2018.
- [11] Zichao Long, Yiping Lu, Xianzhong Ma, and Bin Dong. Pde-net: Learning pdes from data. In *International Conference on Machine Learning*, pages 3208–3216, 2018.
- [12] Yun Long, Xueyuan She, and Saibal Mukhopadhyay. Hybridnet: Integrating model-based and data-driven learning to predict evolution of dynamical systems. In *Conference on Robot Learning*, pages 551–560, 2018.
- [13] Emmanuel de Bezenac, Arthur Pajot, and Patrick Gallinari. Deep learning for physical

processes: Incorporating prior scientific knowledge. *Journal of Statistical Mechanics: Theory and Experiment*, 2019(12):124009, 2019.

[14] Kaiming He, Xiangyu Zhang, Shaoqing Ren, and Jian Sun. Deep residual learning for image recognition. In *Proceedings of the IEEE conference on computer vision and pattern recognition*, pages 770–778, 2016.

[15] Xiaojiao Mao, Chunhua Shen, and Yu-Bin Yang. Image restoration using very deep convolutional encoder-decoder networks with symmetric skip connections. In *Advances in neural information processing systems*, pages 2802–2810, 2016.

[16] Ken-ichi Funahashi and Yuichi Nakamura. Approximation of dynamical systems by continuous time recurrent neural networks. *Neural networks*, 6(6):801–806, 1993.

[17] Xiao-Dong Li, John KL Ho, and Tommy WS Chow. Approximation of dynamical time-variant systems by continuous-time recurrent neural networks. *IEEE Transactions on Circuits and Systems II: Express Briefs*, 52(10):656–660, 2005.

[18] Qianli Liao and Tomaso Poggio. Bridging the gaps between residual learning, recurrent neural networks and visual cortex. *arXiv preprint arXiv:1604.03640*, 2016.

[19] Tian Qi Chen, Yulia Rubanova, Jesse Bettencourt, and David K Duvenaud. Neural ordinary differential equations. In *Advances in neural information processing systems*, pages 6571–6583, 2018.

[20] Adam P Trischler and Gabriele MT D’Eleuterio. Synthesis of recurrent neural networks for dynamical system simulation. *Neural Networks*, 80:67–78, 2016.

[21] Rose Yu, Stephan Zheng, Anima Anandkumar, and Yisong Yue. Long-term forecasting using tensor-train rnns. *arXiv preprint arXiv:1711.00073*, 2017.

[22] Rose Yu, Stephan Zheng, and Yan Liu. Learning chaotic dynamics using tensor recurrent neural networks. In *ICML Workshop on Deep Structured Prediction*, volume 17, 2017.

[23] Kyongmin Yeo and Igor Melnyk. Deep learning algorithm for data-driven simulation of noisy dynamical system. *Journal of Computational Physics*, 376:1212–1231, 2019.

[24] Maziar Raissi and George Em Karniadakis. Hidden physics models: Machine learning of nonlinear partial differential equations. *Journal of Computational Physics*, 357:125–141, 2018.

[25] Maziar Raissi, Paris Perdikaris, and George Em Karniadakis. Physics informed deep learning (part ii): Data-driven discovery of nonlinear partial differential equations, 2017.

[26] Zichao Long, Yiping Lu, and Bin Dong. Pde-net 2.0: Learning pdes from data with a numeric-symbolic hybrid deep network. *Journal of Computational Physics*, 399:108925, 2019.

[27] David E Rumelhart, Geoffrey E Hinton, and Ronald J Williams. Learning representations by back-propagating errors. *Nature*, 323(6088):533–536, 1986.

[28] Paul J Werbos. Backpropagation through time: what it does and how to do it. *Proceedings of the IEEE*, 78(10):1550–1560, 1990.

[29] Mike Schuster and Kuldip K Paliwal. Bidirectional recurrent neural networks. *IEEE Transactions on Signal Processing*, 45(11):2673–2681, 1997.

[30] Barak A Pearlmutter. Learning state space trajectories in recurrent neural networks. *Neural Computation*, 1(2):263–269, 1989.

[31] Tony Robinson. An application of recurrent nets to phone probability estimation. *IEEE transactions on Neural Networks*, 5(2), 1994.

[32] Sepp Hochreiter and Jürgen Schmidhuber. Long short-term memory. *Neural computation*, 9(8):1735–1780, 1997.

[33] E Weinan. A proposal on machine learning via dynamical systems. *Communications in Mathematics and Statistics*, 5(1):1–11, 2017.

- [34] Yiping Lu, Aoxiao Zhong, Quanzheng Li, and Bin Dong. Beyond finite layer neural networks: Bridging deep architectures and numerical differential equations. In *International Conference on Machine Learning*, pages 3282–3291, 2018.
- [35] Bo Chang, Lili Meng, Eldad Haber, Lars Ruthotto, David Begert, and Elliot Holtham. Reversible architectures for arbitrarily deep residual neural networks. In *Thirty-Second AAAI Conference on Artificial Intelligence*, 2018.
- [36] Walter A Strauss. *Partial differential equations: An introduction*. John Wiley & Sons, 2007.

Appendices

A. Configuration Details of the Models

A.1 Residual Encoder-Decoder Network for Source Dynamics

The residual encoder-decoder network for modeling source dynamics comprises three convolutional and three transposed convolutional blocks ($M = 3$). Each convolutional block consists of two convolutional layers and each transposed convolutional block contains two transposed convolutional layers. For all convolution and transposed convolution operations, we use kernels of size 3×3 , which has shown excellent performance in various computer vision tasks. Stride of convolution is set to 2 in the first layer of each convolutional block for downsampling, whereas stride is 1 for the second layers. For symmetricity, stride of the first and second layers of transposed convolutional blocks are set to 1 and 2, respectively. We use 32 feature maps in each convolutional and transposed convolutional layers.

A.2 Baseline Models

Residual Encoder-Decoder Network The configuration of the baseline residual encoder-decoder network (for modeling the combined dynamics) is chosen to be same as the one used for source dynamics. We tested another configuration with $M = 5$; however, that did not contribute to significant performance improvement.

Convolutional LSTM A two-layer convolutional LSTM with each internal state comprising 32 feature maps is used. Kernel size of all convolution operations is set to 5×5 as used in [3].

CNN of PDE-RNN + CNN model A convolutional network with 3 convolutional blocks are used. Each convolutional block consists of two convolutional layers of 32 feature maps. For all convolution operations, we use kernels of size 3×3 .

B. Training Details

Observation maps are normalized to have values within the range $[-1, 1]$. Adam optimizer is used to train the model. We start the training with a stepsize of 0.001 and down-scaled it by 0.99 in every epoch. The model is trained for 200 epochs. The hyperparameter λ associated with source-sparsity loss $\mathcal{L}_{source_sparse}$ is chosen from a range of values between 10^{-8} to 10^{-1} and 0.

All the models are implemented in PyTorch framework. We run all the experiments on a computer equipped with NVIDIA GTX 1080Ti GPU.